

A Synthetic Texas Backbone Power System with Climate-Dependent Spatio-Temporal Correlated Profiles

Jin Lu, *Student Member, IEEE*, and Xingpeng Li, *Senior Member, IEEE*, Hongyi Li, Taher Chegini, Carlos Gamarra, Y. C. Ethan Yang, Margaret Cook, and Gavin Dillingham

Abstract— Most power system test cases only have electrical parameters and can be used only for studies based on a snapshot of system profiles. To facilitate more comprehensive and practical studies, a synthetic power system including spatio-temporal correlated profiles for the entire year of 2019 at one-hour resolution has been created in this work. This system, referred to as the synthetic Texas 123-bus backbone transmission (TX-123BT) system, has very similar temporal and spatial characteristics with the actual Electric Reliability Council of Texas (ERCOT) system. It has a backbone network consisting of only high-voltage transmission lines in Texas, which is obtained by the K-medoids clustering method. The climate data extracted from the North American Land Data Assimilation System (NLDAS) are used to create the climate-dependent profiles of renewable generation and transmission thermal limits. Two climate-dependent models are implemented to determine wind and solar power production profiles respectively. In addition, two sets of climate-dependent dynamic line rating (DLR) profiles are created with the actual climate information: (i) daily DLR and (ii) hourly DLR. Simulation results of security-constrained unit commitment (SCUC) conducted on each of the daily system profiles have validated the developed one-year hourly time series dataset.

Index Terms— Annual power system profiles, backbone transmission topology, climate-dependent renewable models, dynamic line rating, K-medoids clustering, power system operations, security-constrained unit commitment, test power system, transmission line rating.

I. INTRODUCTION

Many power system studies are simulation-based and rely on the synthetic power system test cases due to the limited availability of real system data. These studies cover a wide range of topics including power system stability, reliability, operation, planning, restoration, and state estimation. For example, security-constrained unit commitment (SCUC), security-constrained economic dispatch (SCED), and transmission expansion planning (TEP) are commonly used in power system operational and planning studies [1]-[3]. Restoration and other operation strategies in grid resilience studies also require test case validation [4]-[5]. Generally, a test case in-

cludes all the relevant information for generation, transmission and load. The commonly used test cases are IEEE and CIGRE benchmarks such as the IEEE 118 bus system and CIGRE medium voltage system [6]. Besides these small-scale test power systems, very few large-scale real power system cases are publicly accessible due to the confidentiality of the power industry. To meet the research requirements of large-scale test cases without the access of real large systems, some synthetic test cases are created that resemble the actual systems based on their electrical characteristics. The Polish 2746-bus system is created based on the real power system of Poland [7]. The synthetic grids utilizing the footprint of the western, northeastern, and eastern U.S. regions have been created, and each grid contains more than ten thousand buses [8]. Most existing test cases provide the technical details for steady-state analysis, such as power flow and/or transient-state analysis such as stability simulation. However, these test cases only provide the data for a certain snapshot in time. The long-term time series system profiles are not provided in these test power system cases.

Prior efforts show that power systems will face more climate-related challenges in the 21st century [9]. Despite the new challenges brought by climate change, the performance and mitigation strategy of the climate-impacted power system are not being investigated in depth. To pave the way for these research and industry developments, we have developed a synthetic Texas 123-bus backbone transmission (TX-123BT) system using actual historical climate information to represent the standalone Texas grid within the Electric Reliability Council of Texas (ERCOT) region. The developed TX-123BT system contains the spatio-temporal correlated profiles generated by various climate-dependent models for transmission line rating and renewable generation.

Multiple power system studies such as SCUC on large-scale systems are computationally intensive [10]. To facilitate climate-impact studies and other studies involving large geographical areas and time-sequential data, the test system should focus on the critical backbone transmission network while containing all the essential details of the test case. Hence, the proposed synthetic TX-123BT system has a backbone network topology, which is obtained by the K-medoids clustering method. It has one entire year of data at one-hour resolution with detailed nodal information of all 123 buses in the system.

The created TX-123BT system including its network and generator configurations, spatio-temporal correlated profiles and related climate data have all been published [11]-[12] and can be freely accessed for research purposes. The main contri-

Jin Lu and Xingpeng Li are with the Department of Electrical and Computer Engineering, University of Houston, Houston, TX, 77204, USA (e-mail: jlu28@uh.edu; xingpeng.li@asu.edu).

Hongyi Li and Taher Chegini are with the Department of Civil and Environmental Engineering, University of Houston, Houston, TX, 77204, USA.

Carlos Gamarra, Margaret Cook, and Gavin Dillingham are with Houston Advanced Research Center, Houston, TX, USA.

Y. C. Ethan Yang is with the Department of Civil & Environmental Engineering, Lehigh University, Bethlehem, PA USA.

This work was supported by the Alfred P. Sloan Foundation.

contributions of this paper are as follows,

- The TX-123BT system has a backbone network created by K-medoids clustering. It comprises the essential geographical and electrical information of the unreduced system. The backbone system is time efficient for computation intensive simulations.
- The climate data at all the bus locations in TX-123BT are extracted from North American Land Data Assimilation System (NLDAS) [13]-[14]. It includes air temperature, solar radiation, and wind speed for 2019, and is used to create the climate-dependent time series profiles of the TX-123BT. Hence, the created profiles of solar power, wind power, electrical load, and line thermal rating are spatio-temporal correlated with each other.
- The TX-123BT includes both the hourly and daily dynamic line rating (DLR) profiles. The performances of these two DLR techniques are examined and compared.
- The SCUC simulation is conducted on all the daily profiles in 2019 for validation. The transmission line congestion and locational marginal prices (LMPs) are also analyzed.

The rest of this work is structured as follows. Section II explains the procedures implemented in this work to transform a large-area transmission network into a 123-bus backbone network. Section III presents the generator specifications while section IV presents the climate-dependent renewable production models used for creating renewable production profiles of the TX-123BT. The proposed method for creating the nodal load profiles is described in Section V. Section VI presents the climate-dependent transmission line rating model; the line capacity data representing daily and hourly DLR are also summarized. The SCUC simulation results are analyzed in Section VII. The conclusions are drawn in Section VIII.

II. CLUSTER-BASED BACKBONE NETWORK TOPOLOGY

A bulk power system connects the generation resources and loads with the meshed network including substations and transmission lines. Hence, the power system topology highly depends on the distribution of generation and load, which is related to locational conditions. For example, most large loads are located in/near the cities, and the number of transmission lines in these areas are generally more than other areas.

The synthetic TX-123BT test case is proposed to serve as a benchmark power system for studies on large geography areas, such as analyzing the impact of climate change on power systems. The transmission network in a wide geographical area contains a large number of transmission lines and substations. The complexity of the transmission topology is due to the locally detailed transmission information, which is not necessary for many research topics of interest. Such complexity will increase the computational burden and become an obstacle for most research studies. Hence, we need to reduce the power system topology to relieve the computational burden while retaining critical information.

A typical power system network includes transmission lines at different voltage levels. The transmission lines with higher voltage levels usually have higher capacities and can carry more power flows; in addition, a higher voltage level indicates a longer transmission distance. By extracting the high-voltage

transmission network, we can easily obtain a backbone network that includes almost all the transmission lines with large power flows. We first extract the 345kV backbone transmission network of the synthetic power system based on the footprint of Texas [15]. This creates a 225-bus 345 kV transmission network topology as shown in Fig. 1.

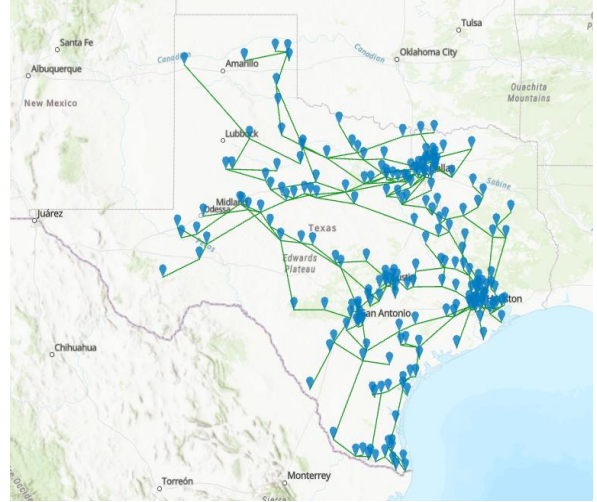


Fig. 1. Illustration of the Texas 225-bus transmission network topology.

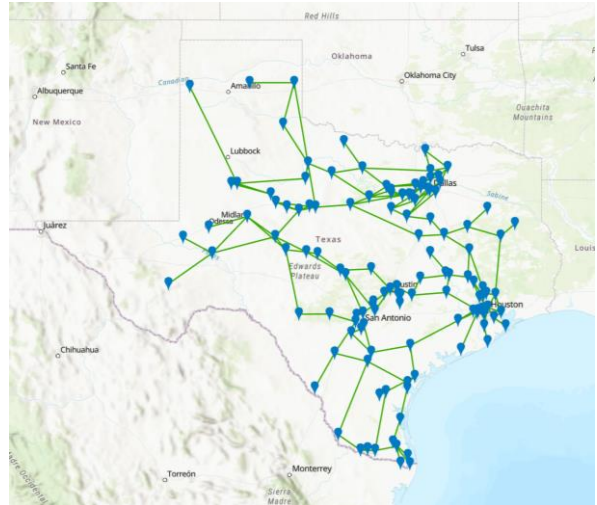


Fig. 2. Illustration of the 123-bus transmission network topology.

For a wide geographical area, the high voltage level transmission network may still include local transmission details, which are unimportant for system-level analysis. Hence, we need to further reduce the data scale while keeping the key information of the test system. Based on different test cases and actual grid data, most short-distance transmission lines are located near the cities. The reactance of these lines is small, and the power flows in these lines are often well below the thermal limits. Therefore, a clustering method should be implemented to aggregate the buses of the 225-bus backbone case. The K-medoids clustering method can find the centroid that is the actual point in the cluster. Also, it is less sensitive to outliers than the typical K-mean clustering method. Using the K-medoids clustering method can better select the backbone buses from the unreduced transmission network which includes buses distributed in remote areas.

The K-medoids clustering algorithm can be described by the following steps: i) randomly select some buses as the initial centroids of clusters; ii) for each bus which is not the centroid, assign it to the cluster whose centroid is closest to it; iii) for each cluster, identify the bus that has the smallest total distance to all other buses in the same cluster as the new centroid of the cluster; iv) if the centroid solution changes, go to step ii; otherwise, stop and report the clustering results.

The distance between two buses is calculated using the haversine formula as shown below.

$$a = \sin^2\left(\frac{\varphi_1 - \varphi_2}{2}\right) + \cos \varphi_1 \cdot \cos \varphi_2 \cdot \sin^2\left(\frac{\lambda_1 - \lambda_2}{2}\right) \quad (1)$$

$$c = 2 \cdot \text{atan2}(\sqrt{a}, \sqrt{1-a}) \quad (2)$$

$$d = R \cdot c \quad (3)$$

where φ represents the latitude of a bus, and λ represents the longitude of a bus. R is the radius of Earth. d is the distance between the two buses.

We created the backbone transmission network topology using the K-medoids clustering method. The transmission network has well-clustered buses. However, some essential buses in remote areas are not included in the backbone network. Hence, we manually add three buses and related lines into the backbone network after a topology comparison with the original 225-bus system. AC power flow simulation is conducted to verify the 123-bus backbone topology. The reduced 123-bus backbone transmission topology is illustrated in Fig. 2, which is very similar to the 225-bus network topology represented by Fig. 1. The major difference is that the 123-bus network has much less buses in the dense city areas. This change can reduce computational complexity in various simulations but does not affect studies such as network congestion analysis.

III. CONVENTIONAL GENERATION PROFILES

A. Generation Fuel Mix

Based on the ERCOT's energy production and generation capacity by fuel types [16]-[17], we can conclude that the major generation fuel types in the ERCOT system are natural gas, wind, coal, nuclear, and solar. In addition, the generation fuel composition may vary in different regions of the ERCOT system. For example, most wind generators are in the northwest of Texas due to the wind source distribution. The TX-123BT system is created to have a very similar system-wide as well as region-wide generation fuel mix with the actual ERCOT system. Based on the generation characteristics of various fuel types for different weather zones and the whole ERCOT [18]-[20], the fuel types of the generators in the TX-123BT system are assigned accordingly and the generator's power capacity is within the capacity range of the corresponding type of generators. In addition, based on the data provided by Energy Information Administration (EIA) [18], ten hydro power plants, each of which is over 10 MW, are also added to the TX-123BT system. Although there are fewer hydro power plants compared to other types of power plants in ERCOT representing a small portion of total generation, they have low opera-

tion costs and high ramping rates which may substantially affect the electricity market and grid reliability.

The statistical data of generation profiles of the developed TX-123BT system are shown in Tables I-II. The system-wide generation fuel mix in the TX-123BT (last row in Table II) is similar to the actual fuel mix provided by ERCOT [21]. Part of the generator's power capacity and fuel type data are shown in Table III. It is worth noting that the renewable generation capacity has grown rapidly in ERCOT. We have adjusted the wind and solar capacity to match the actual ERCOT renewable capacity in 2019.

TABLE I Total Number of Different Fuel Type Generators

Weather Zone	Natural Gas	Wind	Coal	Solar	Nuclear	Hydro
Coast	31	0	2	8	1	0
East	15	0	2	0	0	0
Far West	4	11	0	17	0	0
North	4	9	1	6	0	1
North Central	14	10	4	9	1	1
South	11	18	1	3	0	1
South Central	29	0	3	23	0	6
West	5	34	0	6	0	1
Total	113	82	13	72	2	10

TABLE II Total Capacities (MW) of Different Fuel Type Generators

Weather Zone	Natural Gas	Wind	Coal	Solar	Nuclear	Hydro
Coast	11925	0	2372.5	37.1	2708.6	0
East	6384.6	0	3088.3	0	0	0
Far West	3891.4	2340.6	0	1759.8	0	0
North	2236.1	3989.6	801.0	255.5	0	80
North Central	12093.4	1276.6	4529.2	41.0	2430.0	42
South	7480.3	6716.3	410.0	96.5	0	30.5
South Central	11075.2	0	3559.7	158.6	0	287.3
West	919.6	10156.2	0	130.6	0	58
Total	56005.6	24479.3	14760.7	2479.1	5138.6	497.8

TABLE III Sample of Generator Capacity Profiles in the TX-123BT System

Generator Number	Bus Number	Pmax (MW)	Pmin (MW)	Qmax (MVar)	Qmin (MVar)	Fuel type
1	107	2430	729	894.24	-199.26	Nuclear
6	100	842.5	252.75	392.6	-102.79	Coal
7	100	177.3	53.19	99.29	-11.35	Natural Gas
9	50	1.5	0.45	0	0	Solar
19	32	643.2	0	332.2	0	Wind
283	61	54.9	0	23.5	0	Hydro

B. Conventional Generator Cost & Operation Parameters

1) Coal & Natural Gas Generator

The quadratic function (4) is used to model the thermal power plant's operation cost (c_g). The coefficients C_0 , C_1 and C_2 of typical coal generators and natural gas generators are determined per [22]. The generator startup cost (c_g^{SU}) can be calculated using (5).

$$c_g = C_0 + C_1 * P + C_2 * P^2 \quad (4)$$

$$c_g^{SU} = \eta_g^{SU} * P_g^{Max} * C^F + P_g^{SU} * C_g^O \quad (5)$$

where P_g^{Max} is the generator active power capacity, η_g^{SU} is the startup fuel per unit capacity, C^F is the fuel price, P_g^{SU} is the startup power and C_g^O is another startup cost related to the required startup power.

The coal price used in creating the TX-123BT system is 1.78 \$/MMBtu based on EIA [22]. The annual average natural gas price in Texas is 2.29 \$/Kft³. As the natural gas heat

content is set to be 1000 Btu/ft^3 [23], then the natural gas price becomes $2.29 \text{ \$/MMBtu}$. Based on the above information, the total startup cost is calculated for the coal and natural gas generators in the TX-123BT test system.

In addition, the shutdown costs are also calculated following [19]. The ramping rate, minimum off time, and maximum on time of the coal and natural gas generators are obtained per [20]. The startup time and shutdown time are obtained from [25]. Tables IV through VII show the parameters for representative coal and natural gas generators respectively.

TABLE IV Cost for Various Scale Coal Power Plants

Capacity (MW)	C0 (\$/h)	C1 (\$/h/MW)	C2 (\$/h/MW ²)	Startup Costs (\$/MW Capacity)	Shutdown Costs (\$/MW Capacity)
0-75	0-238	18.28-19.98	0.0016	80-380	8-38
75-150	238-745				
150-350	745-1213				
>350	1213-3043				

TABLE V Other Parameters for Coal Power Plants

Capacity (MW)	Ramping rate (% of the capacity/min)	Startup time (hour)	Shutdown time (hour)	Minimum on time (hour)	Minimum off time (hour)
0-75	0.6-8	4-60	2-60	12	12
75-150					
150-350					
>350					

TABLE VI Cost for Various Scale Natural Gas Power Plants

Capacity (MW)	C0 (\$/h)	C1 (\$/h/MW)	C2 (\$/h/MW ²)	Startup costs (\$/MW Capacity)	Shutdown costs (\$/MW Capacity)
0-400	0-600	23.13-57.03	0.002-0.008	4-80	0.4-8
400-600	600-3859				

TABLE VII Other Parameters for Various Scale Natural Gas Power Plants

Capacity (MW)	Ramping rate (% of the capacity/min)	Startup time (hour)	Shutdown time (hour)	Minimum on time (hour)	Minimum off time (hour)
0-400	0.8-30	5-40	3-40	2	1
400-600					

2) Nuclear Power Plants

Texas has two nuclear power plants. Based on the expense details of nuclear power plants [26], we assume the operation cost of these two Texas nuclear power plants is $17.44 \text{ \$/MWh}$. The nuclear power plants are generally online most of the time. Most nuclear power plants require more than 12 hours to reach full operation, and they can ramp up or down in the load following mode [27]. The parameters of nuclear power plants in the created TX-123BT system are shown in Table VIII.

3) Hydroelectric Power Stations

The average operation cost of hydroelectric power plants is $12.3 \text{ \$/MWh}$ per [28]. We assume the startup and shutdown costs of the hydroelectric power station are zero. Hydroelectric power stations can ramp up rapidly and require much less time

to startup and shutdown. As an example, hydroelectric power plants provided flexible ramping during the generation shortage in Texas in February 2021 [29]. Thus, we assume the startup/shutdown time, minimum on/off time of hydroelectric power stations are zeros.

TABLE VIII Parameters for Nuclear Power Plants

C0 (\$/h)	0	Ramping rate (% of total capacity/min)	5
C1 (\$/h/MW)	17.44	Startup time (hour)	18
C2 (\$/h/(MW) ²)	0	Shutdown time (hour)	18
Startup costs (\$)	1200	Minimum on time (hour)	72
Shutdown costs (\$)	1200	Minimum off time (hour)	72

IV. CLIMATE-DEPENDENT RENEWABLE GENERATION MODELS & PRODUCTION PROFILES

A. Climate-Dependent Wind Model and Production Profiles

To create the backbone TX-123BT case profiles that depend on the climate variables, we first obtain the climate data from the Phase 2 of the North American Land Data Assimilation System (NLDAS-2) [13]-[14]. The NLDAS-2 climate dataset includes the shortwave/longwave solar radiation, air temperature and wind speed near the ground surface with a one-hour resolution. Since this paper aims to create the time-series profiles that resemble the ERCOT in 2019, the historical climate data for all the hours in 2019 are extracted.

In the ERCOT system, the full capacity up to the high sustained limit (HSL) of wind generation resources is considered available to be dispatched in the reliability unit commitment (RUC) [30]. However, ERCOT only provides limited data for the HSL in the current operating plan (COP), which is not the actual HSL. Instead of determining the wind hourly HSL for daily grid operations, we use the wind hourly production data [31] to create the wind profiles.

The available wind power output can be calculated using (6)-(7) when wind speed is between the cut-in speed and rated-speed. V is the wind speed, ρ is the air density, C_p is the wind turbine efficiency, A is the turbine blade swept area, and D is the turbine diameter. For all the wind turbines in the TX-123BT system, the cut-in speed is set to 3.5m/s , the rated speed is set to 13m/s , and the cut-out speed is set to 25m/s .

$$P^{W,Max} = \frac{1}{2} \cdot \rho \cdot A \cdot V^3 \cdot C_p \quad (6)$$

$$A = \frac{\pi}{4} \cdot D^2 \quad (7)$$

The extracted historical wind speed data in NLDAS-2 is the measured wind speed at 10m height and most wind turbines on land are about 80m high [32]. To determine wind speed at 80m , we use log wind profile [33] to estimate the wind speed at the wind turbines' height. The equation for the log wind profile is shown below.

$$u(z_2) = u(z_1) \cdot \frac{\ln((z_2 - d)/z_0)}{\ln((z_1 - d)/z_0)} \quad (8)$$

The wind speeds at two different heights z_1 and z_2 are represented by $u(z_1)$ and $u(z_2)$ respectively. Zero-plane displacement d is the height that zero-wind speed is achieved because of flow obstacles. It can be approximated as $2/3$ to $3/4$ of the average height of the obstacles [33]. Roughness length

z_0 is the roughness of the surface. Based on the terrain of Texas, z_0 is set to 0.3 and d is set to 6. The wind speed at 80m is about 2.13 times of wind speed at 10m.

To create more practical climate-dependent wind production profiles, the capacities and geographic locations of the wind power plants in the TX-123BT should be close to the actual ERCOT system. The wind plant capacities in the TX-123BT system are adjusted to match the actual ERCOT wind generation in 2019 using the least square method, as described by (9)–(14).

$$\min \sum_h^H \left(\sum_i^{N^W} p_{i,h}^{W,Case} - p_h^{ERCOT} \right)^2 \quad (9)$$

$$P_{i,h}^{W,Case} = k_{i,h}^W \cdot C_i^W \cdot V_{i,h}^3 \quad \forall i \in N^W, h \in H \quad (10)$$

$$k_{i,h}^W = k_{i,h+24}^W \quad \forall i \in N^W, h \in H \quad (11)$$

$$-0.0001 \leq k_{i,h}^W - k_{i,h-1}^W \leq 0.0001 \quad \forall i \in N^W, h \in H \quad (12)$$

$$-50 \leq C_i^W - C_i^{W0} \leq 50 \quad \forall i \in N^W, h \in H \quad (13)$$

$$C_i^W \geq 0 \quad \forall i \in N^W \quad (14)$$

The least square method can adjust the wind power plant capacities in the TX-123BT to minimize the square error between the wind production of the TX-123BT and the ERCOT per (9). $p_{i,h}^{W,Case}$ is the power output of wind farm i in hour h in the TX-123BT. p_h^{ERCOT} is the total wind output power of the actual ERCOT system in hour h . Hour h is an hour in 2019. The aggregated wind power production in a wind farm is related to the adjusted capacity of wind farm C_i^W and the wind speed $V_{i,h}$ per (10).

The wind turbine coefficient k is a comprehensive coefficient considering various factors including the wind direction and wind turbine efficiency. The wind turbine coefficient k is assumed to be a constant for a specific wind turbine for each hour of the day per (11). The changing magnitude of k is limited to 0.0001 over two consecutive hours. Besides, the adjustment of the capacity for each wind farm in TX-123BT is less than 50MW per (13). The adjusted wind capacity should be non-negative per (14). The least square method can find the most realistic wind turbine coefficients and capacities for wind farms in the TX-123BT system.

The created wind production hourly time series profiles are compared to the corresponding real ERCOT wind production in 2019 in Fig. 3. The mean hourly wind power profile (within a day), averaged over 365 days in 2019, is compared to the actual ERCOT hourly statistics in Fig. 4. According to the comparison, we can conclude that the created wind production profiles are very similar to the actual situation. The hourly wind power production from seven wind farms at bus 119 on January 3, 2019, is illustrated in Fig. 5. We can observe that each wind plant's production varies according to the wind speed on bus 119.

B. Climate-Dependent Solar Model and Production Profiles

A five-parameter single diode equivalent circuit is commonly used and suitable for PV cell, module and array [34]. In [35], the operation condition variables (temperature, radiation, and air mass) are used in a five-parameter equation. Since we

are mainly interested in the maximum available solar power output at different radiation and temperature, we can calculate the maximum power point using (15) [36]–[37].

$$P_{mp} = \frac{E_e}{E_0} \cdot P_{mp0} \cdot [1 + \gamma \cdot (T_c - T_0)] \quad (15)$$

where P_{mp} is the maximum power output for the certain operation condition. E_e and T_c are the effective radiation and temperature on the solar cells respectively. P_{mp0} is the maximum power output at the standard testing condition (STC). E_0 and T_0 are the radiation and temperature at STC respectively. γ is the temperature coefficient that indicates the influence of the temperature on the solar power transfer efficiency.

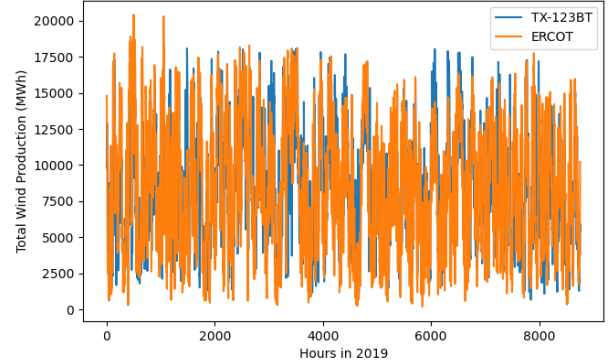


Fig. 3. Wind power production for all hours in 2019.

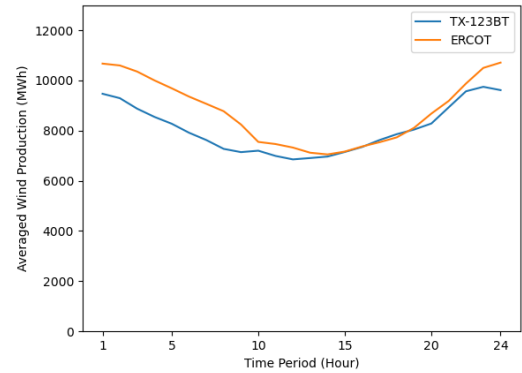


Fig. 4. Hourly wind power profiles comparison.

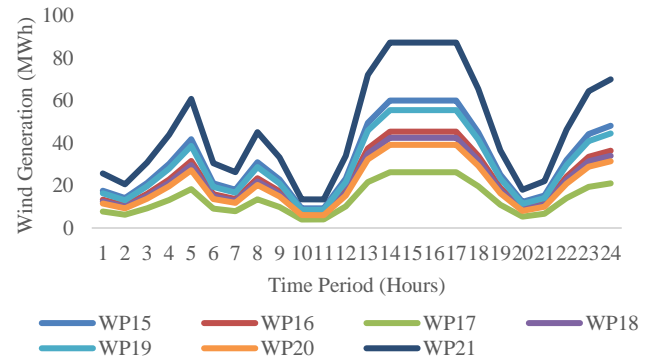


Fig. 5. Output power of seven wind plants (WP) on January 3, 2019.

The NLDAS-2 provides the historical data for shortwave and longwave solar radiation flux downwards. Based on the widely used solar panel's spectral response range, we use the radiation flux downwards to estimate the effective solar radi-

tion on the solar panels. We also estimate the solar cell temperature using the ambient air temperature at the corresponding solar panel.

Based on the processed climate data and solar power production model, the solar power production for all the solar farms in the TX-123BT system is calculated. The system-wide hourly solar production of the TX-123BT is compared with ERCOT solar production in 2022 (the historical data of 2019 is not accessible). The hourly solar productions averaged over all the days in Quarter 1 for the synthetic TX-123BT system and the actual ERCOT system are shown in Fig. 6. We can observe that the deviation is within a reasonable range. The hourly solar power production for four solar farms in TX-123BT is shown in Fig. 7.

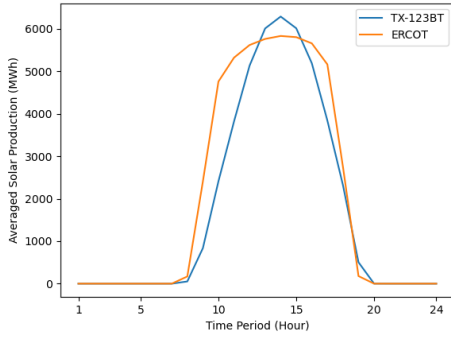


Fig. 6. Averaged hourly solar power production in Quarter 1.

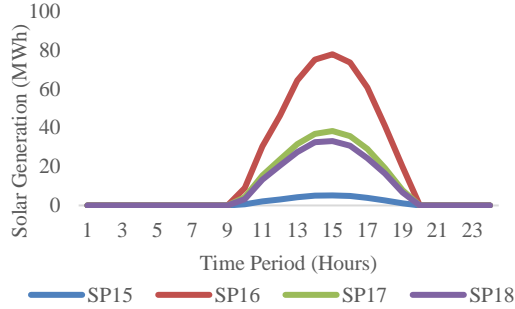


Fig. 7. Hourly power output of four solar plants (SP) on January 1, 2019.

V. CREATION OF LOAD PROFILES

The ERCOT historical load data [38] includes the hourly total load in each weather zone for all hours in 2019. The hourly load profiles at the nodal level are created for the TX-123BT system such that they match the total zonal load amount in each weather zone for each hour in 2019. Part of the load profiles are illustrated in Table IX.

TABLE IX Sample Load Profiles for Different Hours on December 31, 2019

Bus Number	Hour 1	Hour 5	Hour 9	Hour 13	Hour 17	Hour 21
Bus 1	96.51	102.39	118.19	91.76	84.25	96.28
Bus 2	97.86	103.56	116.47	95.4	87.29	97.41
Bus 3	171.3	172.01	173.67	161.79	158.4	165.91
Bus 4	198.59	202.18	231.79	213.28	208.4	212.48
Bus 5	25.58	24.5	28.54	28.53	28.73	28.21
Bus 6	606.36	641.1	754.35	608.1	555.7	613.43
Bus 7	42.61	45.05	53.01	42.73	39.05	43.11

VI. CLIMATE-DEPENDENT TRANSMISSION LINE RATING

The transmission line thermal capacity in the three-phase system can be calculated given the line ampacity and line voltage. The IEEE Std 738-2012 [39] is used to calculate the ampacity of lines at different temperature, solar radiation and wind speed conditions. The detailed calculation is described by (16)-(23).

$$q_c + q_r = q_s + I^2 \cdot R(T_{avg}) \quad (16)$$

$$I = \sqrt{\frac{q_c + q_r - q_s}{R(T_{avg})}} \quad (17)$$

$$q_{c1} = K_{angle} \cdot [1.01 + 1.35 \cdot N_{Re}^{0.52}] \cdot k_f \cdot (T_s - T_a) \quad (18)$$

$$q_{c2} = K_{angle} \cdot 0.754 \cdot N_{Re}^{0.6} \cdot k_f \cdot (T_s - T_a) \quad (19)$$

$$K_{angle} = 1.194 - \cos(\varphi) + 0.194 \cdot \cos(2\varphi) + 0.368 \cdot \sin(2\varphi) \quad (20)$$

$$q_r = 17.8 \cdot D_0 \cdot \varepsilon \cdot \left[\left(\frac{T_s + 273}{100} \right)^4 - \left(\frac{T_a + 273}{100} \right)^4 \right] \quad (21)$$

$$q_s = \alpha \cdot Q_{se} \cdot \sin(\theta) \cdot A' \quad (22)$$

$$\theta = \cos^{-1}[\cos(H_c) \cdot \cos(Z_c - Z_l)] \quad (23)$$

Equation (16) is the heat balance equation of the conductor. q_c is the convective heat loss. q_r is the radiated heat loss rate. q_s is the rate of solar heat gain. I is the current in the conductor and $R(T_{avg})$ is the conductor resistance at temperature T_{avg} , which is the average temperature in the conductor. (16) can be transformed into (17), which can be used to calculate the current in the conductor at the conductor maximum temperature. In (18)-(20), q_{c1} and q_{c2} are the forced convection and the higher value of q_{c1} and q_{c2} will be used as the value of q_c . N_{Re} is the dimensionless Reynolds number. K_f is the thermal conductivity of air. T_s is the conductor surface temperature, and T_a is the ambient temperature. K_{angle} is wind direction factor and φ is the angle between the wind direction and the conductor axis. In (21), the radiated heat loss is related to the diameter of the conductor D_0 , the emissivity ε , the conductor surface temperature T_s , and ambient temperature T_a . The rate of solar heat gain can be calculated by (22). α is the solar absorptivity. Q_{se} is total solar and sky radiated heat intensity corrected for the elevation. A' is the projected area of the conductor. θ is the effective angle of incidence of the sun's rays. In (23), θ is determined by the altitude of the sun H_c , the azimuth of the sun Z_c , and the azimuth of the line Z_l .

There are three types of aluminium conductor steel reinforced (ACSR) conductors used for the transmission lines in the TX-123BT system: Kiwi, Bobolink and Finch. Different types of ACSR conductors have different conductor diameters and resistances versus temperature characteristics. We use the linear approximation as shown in (24) for determining the conductor resistance at a certain temperature. $R(T_{high})$ and $R(T_{low})$ are the conductor resistance at temperature T_{high} and T_{low} respectively.

$$R(T_{avg}) = \left[\frac{R(T_{high}) - R(T_{low})}{T_{high} - T_{low}} \right] \cdot (T_{high} - T_{low}) + R(T_{low}) \quad (24)$$

Although the extracted historical climate data have detailed nodal information at one-hour resolution, they do not perfectly meet the needs of transmission line calculation. Several assumptions are made as follows. First, the line ambient temperature is assumed to be the same as the temperature 2 meters above ground. Second, since most long-distance transmission lines are overhead lines and the transmission towers are generally 55-150 feet (16.8m-45.72m), the wind speed at the transmission line's height is estimated using the aforementioned log wind profile method. Third, the angle between the wind direction and the transmission line is assumed to be 45-degrees. The wind speed perpendicular to the conductor V_w can be calculated using (25)-(26). In (25), V_z and V_m is the zonal and meridional wind speed extracted from NLDAS. V_{wind} is the composite speed.

$$V_{wind} = \sqrt{V_z^2 + V_m^2} \quad (25)$$

$$V_w = V_{wind} * \sin(45^\circ) \quad (26)$$

The total heat intensity corrected for elevation Q_{se} is calculated using (27)-(29) per the IEEE Std 738-2012.

$$Q_s = A + B \cdot H_c + C \cdot H_c^2 + D \cdot H_c^3 + E \cdot H_c^4 + F \cdot H_c^5 + G \cdot H_c^6 \quad (27)$$

$$Q_{se} = K_{solar} \cdot Q_s \quad (28)$$

$$K_{solar} = A + B \cdot H_e + C \cdot H_e^2 \quad (29)$$

In (27)-(29), Q_s is the total heat flux density by a surface at sea level. K_{solar} is the elevation corrective factor. A , B , C , D , E , F , and G are polynomial coefficients.

The total heat flux by the Earth's surface Q_s is assumed to be the summation of the downward shortwave radiation Q_{short} and longwave radiation Q_{long} , which are the data extracted from NLDAS. Radiation from the Earth's surface is omitted. Thus, Q_s can be calculated using (30).

$$Q_s = Q_{short} + Q_{long} \quad (30)$$

In the calculation, the environmental parameters are determined based on the actual Texas conditions. The altitude and azimuth of the sun at noon are used in the calculation. The altitude of the sun H_c is calculated based on the average latitude of Texas which is 30.5° N. The elevation of the conductor above the sea level H_e is set to Texas average elevation. For ACSR transmission lines, the common continuous operational maximum temperature is 90°C. The parameters for the Texas line ampacity calculation are listed in Table X.

Dynamic line rating is an effective strategy in power system operations to fully utilize the available transmission capacity of the lines under various environmental conditions. In this paper, we have created two profiles using the daily DLR and the hourly DLR, respectively.

The daily DLR profile has the same fixed line ratings in the entire day, which is used by many power system operators. We use the highest hourly temperature, solar radiation, and the lowest hourly wind speed as the environmental values in the daily line rating calculation. The daily line rating profiles are calculated for all the days in 2019 respectively. The daily thermal ratings of line 15 during the year 2019 are shown as an example in Fig. 8.

TABLE X Some Input Data for Texas Line Ampacity Calculation

H_c	The altitude of the sun	30.5	deg
Z_c	The azimuth of the sun	180	deg
H_e	The elevation of conductor above sea level	520	m
ϵ	The emissivity	0.8	-
α	Solar absorption	0.8	-
μ_f	The air viscosity	2.04e-5	-
T_{film}	Average temperature of the boundary layer	70	°C
K_f	The thermal conductivity of air	0.0295	W/m·°C
T_c	The conductor maximum temperature	90	°C

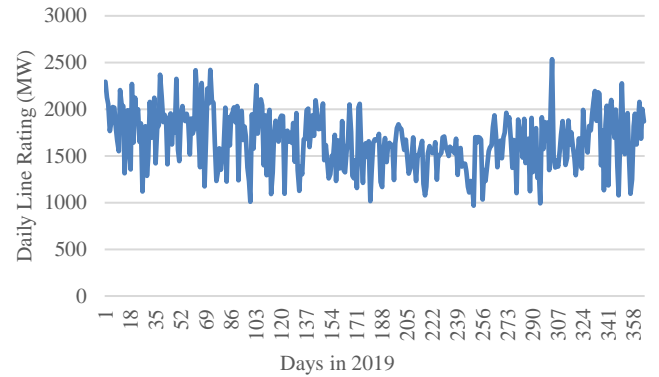


Fig. 8. The daily thermal ratings of line 15 during the year 2019.

The hourly line rating method can capture the suitable line ratings for each hour in the daily operation. Each hour's temperature, solar radiation, and wind speed are used in the line rating calculation for the corresponding hour. Hourly line ratings are higher than the daily line rating in most instances. Hence, using hourly line rating can reduce operational costs and improve system operational efficiency. The hourly line ratings are calculated for all the hours in 2019. The hourly thermal ratings of line 15 in four days for different quarters are shown in Fig. 9.

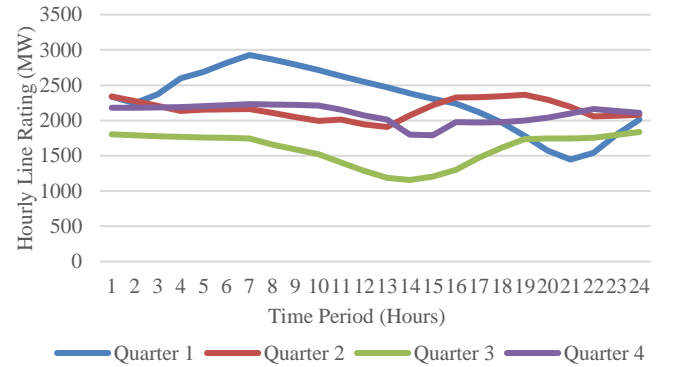


Fig. 9. Thermal ratings of line 15 in four typical days for different quarters.

VII. SCUC SIMULATION AND ANALYSIS

A. SCUC model

To analyze the daily operational conditions of the created TX-123BT system, a standard SCUC model in [40] is used

and simulation is conducted on the TX-123BT. The objective of the daily operational model is to minimize the total cost of the power system, which includes the generator operation cost, no-load cost and startup cost. The generator related constraints such as maximum output, reserve, and ramping constraints are included. The line flow equation and nodal power balance equation are also included. In the SCUC model, the line thermal limit for fixed line rating during a day is shown in (31).

$$-P_k^{max} \leq P_{kt} \leq P_k^{max} \quad \forall k, t \quad (31)$$

The SCUC simulations are conducted to verify all 365 daily system profiles of the TX-123BT test case with daily line ratings. The SCUC optimization problems are feasible for all daily profiles without any load shedding. Since the renewable production, line rating and loads are different in those 365 daily profiles, the feasibility of SCUC optimization problems for all the daily profiles can validate that the created test system is practical and reliable.

B. Comparison of the Electricity Market

Since the locational marginal prices (LMPs) can be obtained from the SCUC simulations, the electricity market results of the TX-123BT and actual ERCOT can be compared.

1) Actual ERCOT Electricity Market

Electricity prices are affected by many factors and one year's price data may not well reflect the actual electricity market. Hence, we collect and analyze the day ahead market (DAM) price data in a 5-year period (2015-2019). After observing DAM prices for different hours and load zones under different scenarios, some characteristics of the actual ERCOT electricity prices are observed and summarized as follows,

- The electricity prices on weekends are usually lower than the prices on weekdays.
- Quarter 3 has the highest electricity price while Quarter 1 has the lowest electricity price.
- The electricity prices at different load zones are slightly different during off-peak hours, but the electricity prices usually have larger locational variety during peak hours, especially in Quarter 3.
- For the peak hours around 15:00-18:00, the electricity prices are much higher than the off-peak hour prices in Quarter 3.

2) Synthetic TX-123BT Electricity Market

The LMPs of the TX-123BT are obtained using the dual variables of the nodal power balance constraints in SCUC simulation. After the analysis of the TX-123BT LMPs and the ERCOT DAM prices, we conclude that the two systems have very similar nodal electricity prices range under different scenarios, which is shown in Table XI.

The system-wide electricity prices for different typical seasonal days are shown in Figs. 10a-10d. We can observe that, in Quarters 3, the electricity prices are higher than in Quarters 1. This disparity can be explained by the larger demands in Quarters 3. The high demands require generators which are more expensive for electricity production to come online, resulting in higher electricity prices in these quarters.

The day with the highest load among all the days in 2019 is selected as the peak load day. Two scatter plots of nodal LMPs for the normal load day and peak load day are shown in Fig. 11 – Fig. 12. From the simulation results, we can con-

clude that the electricity prices at different load zones are slightly different during low load demand scenarios (for most buses). However, the electricity prices locational variety is large during peak hours in Quarter 3. The characteristics of the LMPs are in line with the actual ERCOT electricity price characteristics that we summarized in the above subsection.

TABLE XI Electricity Price Range Under Different Scenarios

Scenario	Trough Hour	Normal Hour	Peak Hour
Quarter 1, Weekday	15-24	24-30	30-45
Quarter 1, Weekend	15-20	20-25	25-33
Quarter 2, Weekday	16-25	25-35	35-55
Quarter 2, Weekend	16-25	25-30	30-50
Quarter 3, Weekday	18-25	25-50	50-220
Quarter 3, Weekend	18-25	25-45	45-110
Quarter 4, Weekday	17-25	25-30	30-40
Quarter 4, Weekend	15-24	24-28	28-45

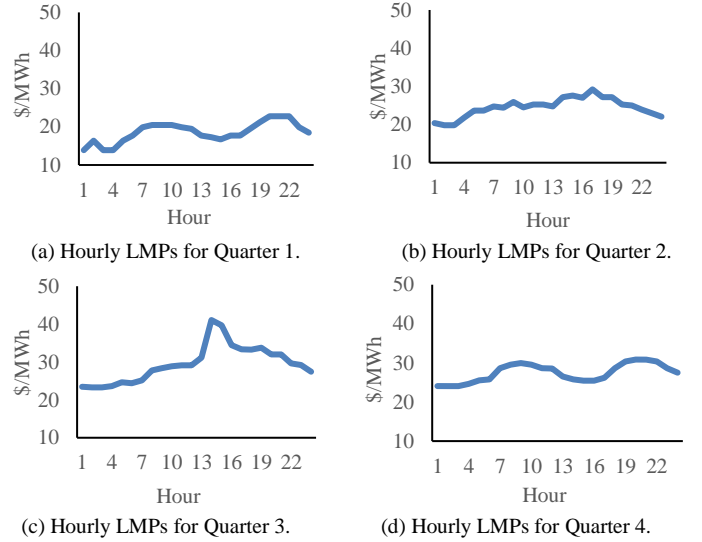


Fig. 10. Daily electricity prices for different quarters.

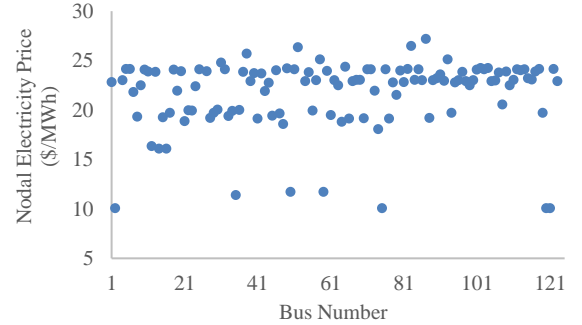


Fig. 11. Nodal LMPs for Hour 15 in a normal load day.

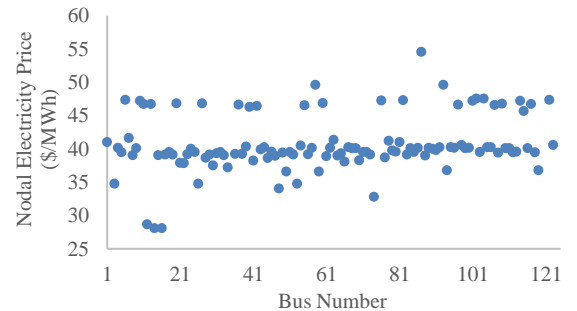


Fig. 12. Nodal LMPs for Hour 15 in the peak load day.

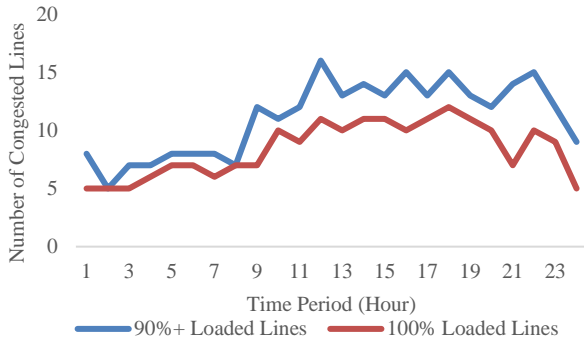


Fig. 13. Number of congested lines during the peak load day.

C. Peak Load Scenarios and Line Congestion Analysis

Congested lines are classified based on the power flow results of the SCUC simulations. Two types of congested lines are classified: (i) 100% loaded lines and (ii) 90%+ loaded lines. The 100% loaded lines are the transmission lines on which the active power flow is 100% of the line capacity. The 90%+ loaded lines are the transmission lines on which the active power flow is over 90% but less than 100% of the line capacity.

The numbers of congested lines at different hours during the peak load day are shown in Fig. 13. We can observe that more transmission lines are congested in the peak hours.

D. DLR Performance Analysis

The SCUC simulation is also conducted on the TX-123BT with hourly DLR profiles. The line thermal limit constraint (32) is replaced by the following constraint since the line limits P_{kt}^{max} are now different for different hours and need an extra index of time interval t .

$$-P_{kt}^{max} \leq P_{kt} \leq P_{kt}^{max} \quad \forall k, t \quad (32)$$

The SCUC simulation results including total operational cost, renewable generation, LMPs, and transmission congestion, are analyzed and compared with SCUC using daily DLR profiles. The overall numerical results are shown in Table XII.

TABLE XII SCUC Simulation Results for a Normal Day in Quarter 2

Numerical Results	Daily DLR	Hourly DLR
Total Operational Cost (\$)	8.09M	7.95M (-1.7%)
Total Renewable Generation (GWh)	271.95	275.48 (+1.3%)
Average LMPs (\$/MWh)	18.66	17.98 (-3.6%)
ANCLPH	6.9	8.2

ANCLPH denotes the average number of congestion lines per hour.

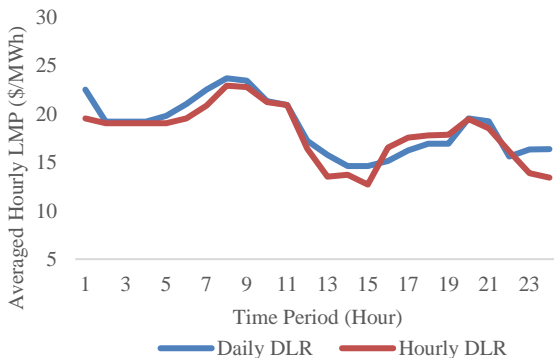


Fig. 14. Hourly average LMPs for a normal day in Quarter 2.

The total operational cost of the hourly DLR case is lower than the daily line rating case, and the cost saving is about 1.7% with hourly DLR. One reason is that the increased transmission capacity can relieve network congestion and reduce the curtailment of renewable energy that has a much lower (zero) cost than the conventional generation. The average LMP of the hourly DLR case is also lower than the case using conservative daily DLR. The systemwide average LMPs for a normal day in Quarter 2 are shown in Fig. 14. We can observe that the average LMPs of hourly DLR is lower than the LMPs of daily DLR for majority of the hours.

VIII. CONCLUSION

In this paper, we present the methods and implementation details to create the synthetic TX-123BT test system, which covers the wide geographical area of Texas. The created test case has reduced system size while retaining geographical characteristics. Hence, the test case is suitable for power system studies that require geographical information and less computational burden.

The hourly climate data in NLDAS-2, including solar radiation, air temperature and wind speed for all the 123 bus locations are extracted and utilized. Using the climate-dependent models for solar/wind production and transmission line rating, the associated spatio-temporal correlated profiles of the TX-123BT are created. The time series nodal load profiles are also created in a way to match the actual zonal load for each of the eight weather zones in ERCOT for each hour in the entire year of 2019. The created TX-123BT system with both daily DLR and hourly DLR profiles is validated through SCUC simulations. The SCUC results in peak load scenarios and the comparison between the conservative daily DLR and hourly DLR are also discussed in this paper, demonstrating the effectiveness and practicality of the created synthetic TX-123BT system for facilitating the research and studies in various power system areas. Since it covers a period of one entire year at one-hour resolution with strong practical spatiotemporal correlations embedded in the dataset, it would also facilitate power system studies involving machine learning such as reinforcement learning and graph neural networks [42]-[43].

REFERENCES

- [1] A. V. Ramesh, X. Li and K. W. Hedman, "An Accelerated-Decomposition Approach for Security-Constrained Unit Commitment with Corrective Network Reconfiguration," *IEEE Transactions on Power Systems*, vol. 37, no. 2, pp. 887-900, Mar. 2022.
- [2] Z. Xin-gang, L. Ji, M. Jin, and Z. Ying, "An improved quantum particle swarm optimization algorithm for Environmental Economic Dispatch," *Expert Systems with Applications*, vol. 152, p. 113370, 2020.
- [3] X. Li and Q. Xia, "Power System Expansion Planning with Seasonal Network Optimization," *Innovative Smart Grid Technologies (ISGT)*, Washington D.C., USA, Feb. 2020.
- [4] J. Lu and X. Li, "Optimal skeleton network reconfiguration considering topological characteristics and transmission path," *53rd North American Power Symposium (NAPS)*, 2021.
- [5] N. Bhusal, M. Abdelmalak, M. Kamruzzaman, and M. Benidris, "Power system resilience: Current practices, challenges, and future directions," *IEEE Access*, vol. 8, pp. 18064-18086, 2020.
- [6] S. Peyghami, P. Davari, M. Fotuhi-Firuzabad, and F. Blaabjerg, "Standard Test Systems for Modern Power System Analysis: An overview," *IEEE Industrial Electronics Magazine*, vol. 13, no. 4, pp. 86-105, 2019.
- [7] J. Snodgrass, S. Kunkolienkar, U. Habiba, Y. Liu, M. Stevens, F. Safdarian, T. Overbye, and R. Korab, "Case study of enhancing the

- MATPOWER Polish Electric Grid,” *IEEE Texas Power and Energy Conference (TPEC)*, 2022.
- [8] Texas A&M University Electric grid test case repository. <https://electricgrids.engr.tamu.edu/electric-grid-test-cases/>
- [9] H. Shakouri G. and S. Aliakbarisani, “At what valuation of sustainability can we abandon fossil fuels? A comprehensive multistage decision support model for Electricity Planning,” *Energy*, vol. 107, pp. 60–77, 2016.
- [10] A. V. Ramesh and X. Li, “Machine Learning Assisted Model Reduction for Security-Constrained Unit Commitment”, *54th North American Power Symposium*, Salt Lake City, UT, USA, Oct. 2022.
- [11] Renewable Power Grid Lab, University of Houston, “Resources / Synthetic Texas 345kV Backbone Transmission System (TX-123BT) with Climate-Dependent Spatio-Temporal Correlated Profiles”, [Online]. Available at: <https://rpglab.github.io/resources/TX-123BT/>
- [12] J. Lu and X. Li, “Texas Synthetic Power System Test Case (TX-123BT).zip”. *figshare*, 23-Feb-2023, doi: 10.6084/m9.figshare.22144616.
- [13] Y. Xia, B. A. Cosgrove, M. B. Ek, J. Sheffield, L. Luo, E. F. Wood, and K. Mo, “Overview of the north american land data assimilation system (NLDAS),” *Land Surface Observation, Modeling and Data Assimilation*, pp. 337–377, 2013.
- [14] README Document for North American Land Data Assimilation System Phase 2 (NLDAS-2) Products. <https://hydro1.gesdisc.eosdis.nasa.gov/data/NLDAS/README.NLDAS2.pdf>
- [15] A.B. Birchfield, T. Xu, K.M. Gegner, K.S. Shetye, T.J. Overbye, “Grid Structural Characteristics as Validation Criteria for Synthetic Networks,” *IEEE Transactions on Power Systems*, vol. 32, no. 4, pp. 3258–3265, July 2017.
- [16] ERCOT report for interval generation by fuel. <http://www.ercot.com/content/wcm/lists/181766/IntGenbyFuel2021.xlsx>
- [17] ERCOT winter capacity by fuel type. <https://www.spglobal.com/marketintelligence/en/news-insights/latest-news-headlines/as-texas-digs-out-plans-proceed-to-add-35-gw-of-solar-wind-capacity-to-grid-62719521>
- [18] The U.S. generators fuel type data by EIA: <https://www.eia.gov/state/maps.php>
- [19] T. Xu, A. B. Birchfield, K. M. Gegner, K. S. Shetye, and T. J. Overbye, “Application of large-scale synthetic power system models for Energy Economic Studies,” *Proceedings of the 50th Hawaii International Conference on System Sciences (2017)*, 2017.
- [20] “Gas Power Plant Fuel Requirements and uncertainty considering increasing renewables penetration,” [Online]. Available: <https://www.researchgate.net/profile/Jarrad-Wright/publication>.
- [21] ERCOT, Bill Magness, President & Chief Executive Officer of ERCOT, “Review of February 2021 Extreme Cold Weather Event – ERCOT Presentation”, *Urgent Board of Directors Meeting*, Feb. 24, 2021.
- [22] Average cost of coal delivered for electricity generation by EIA. https://www.eia.gov/electricity/monthly/xls/table_4_10_a.xlsx
- [23] Texas heat content of natural gas by EIA. https://www.eia.gov/dnav/ng/hist/nga_epg0_vgth_stx_btucfa.htm
- [24] D. Krishnamurthy, W. Li and L. Tefsatsion, “An 8-Zone Test System Based on ISO New England Data: Development and Application,” in *IEEE Transactions on Power Systems*, vol. 31, no. 1, pp. 234–246, Jan. 2016.
- [25] Power plant cycling cost by NREL: <https://www.nrel.gov/docs/fy12osti/55433.pdf>
- [26] Average Power Plant Operating Expenses for Major U.S. Investor-Owned Electric Utilities by EIA. https://www.eia.gov/electricity/annual/html/epa_08_04.html
- [27] Technical and Economic Aspects of Load Following with Nuclear Power Plants by OECD. <https://www.oecd-neo.org/ndd/reports/2011/load-following-npp.pdf>
- [28] Published by Statista Research Department, “U.S. hydroelectric power plant operating expenses 2021,” *Statista*.
- [29] Y. R. Glazer, D. M. Tremaine, J. L. Banner, M. Cook et al., “Winter storm Uri: A test of Texas’ water infrastructure and water resource resilience to extreme winter weather events,” *Journal of Extreme Events*, vol. 08, no. 04, 2021.
- [30] “Optimizing Wind Generation in ERCOT Nodal Market”, *FERC Conference on Increasing Real-Time and Day-Ahead Market Efficiency through Improved Software*, June 2014.
- [31] ERCOT Hourly Aggregated Wind Output. <https://www.ercot.com/misapp/GetReports.do?reportTypeId=13424&reportTitle=Hourly%20Aggregated%20Wind%20Output&showHTMLView=&mimicKey>
- [32] J. Gerdes, “Kissing the sky: The Pros and cons of Ultra-Tall Wind Turbine Towers,” *Greentech Media*, 05-Sep-2019. [Online]. Available: <https://www.greentechmedia.com/articles/read/the-pros-and-cons-of-ultra-tall-wind-turbine-towers>.
- [33] J. D. Holmes and S. Bekele, *Wind loading of structures*. Boca Raton: CRC Press, 2022.
- [34] J.L. Gray, “The Physics of the Solar Cell,” *Handbook of Photovoltaic Science and Engineering*, 2011.
- [35] W. De Soto, S. A. Klein, and W. A. Beckman, “Improvement and validation of a model for photovoltaic array performance,” *Solar Energy*, vol. 80, no. 1, pp. 78–88, 2006.
- [36] NREL PVWatts calculator. <https://pvwatts.nrel.gov/>
- [37] NREL PVWatts Version 5 Manual. <https://www.nrel.gov/docs/fy14osti/62641.pdf>
- [38] 2019 ERCOT hourly load data. http://www.ercot.com/gridinfo/load/load_hist
- [39] “IEEE Standard for Calculating the Current-Temperature Relationship of Bare Overhead Conductors,” *IEEE Std 738-2012*, pp.1-72, Dec. 2013.
- [40] J. Lu and X. Li, “The Benefits of Hydrogen Energy Transmission and Conversion Systems to the Renewable Power Grids: Day-ahead Unit Commitment”, *54th North American Power Symposium*, Oct. 2022.
- [41] ERCOT day-ahead market historical data. <https://www.ercot.com/mktinfo/dam>.
- [42] T. Pham and X. Li, “Reduced Optimal Power Flow Using Graph Neural Network”, *54th North American Power Symposium*, Salt Lake City, UT, USA, Oct. 2022.
- [43] M. Tuo and X. Li, “Deep Learning based Security-Constrained Unit Commitment Considering Locational Frequency Stability in Low-Inertia Power Systems”, *54th North American Power Symposium*, Salt Lake City, UT, USA, Oct. 2022.